

The Gamma Generalized Normal Distribution: A Descriptor of SAR Imagery

G. M. Cordeiro* R. J. Cintra† L. C. Rêgo‡ A. D. C. Nascimento*

Abstract

We propose a new four-parameter distribution for modeling synthetic aperture radar (SAR) imagery named the gamma generalized normal (GGN) by combining the gamma and generalized normal distributions. A mathematical characterization of the new distribution is provided by identifying the limit behavior and by calculating the density and moment expansions. The GGN model performance is evaluated on both synthetic and actual data and, for that, maximum likelihood estimation and random number generation are discussed. The proposed distribution is compared with the beta generalized normal distribution (BGN), which has already shown to appropriately represent SAR imagery. The performance of these two distributions are measured by means of statistics which provide evidence that the GGN can outperform the BGN distribution in some contexts.

Keywords

Gamma generalized distribution, Generalized normal, Maximum likelihood, Moment, SAR images.

1 Introduction

The statistics literature is filled with hundreds of continuous univariate distributions and several recent developments focus on new techniques for building meaningful distributions. Numerous classical distributions have been extensively used over the last decades for modeling data in several areas such as biological studies, environmental sciences, engineering, economics, actuarial sciences, finance, demography, insurance and medical sciences. However, in many applied areas such as image processing, finance and insurance data, there is a clear need for extended forms of these distributions. Two core reasons are:

- a) The proposal of extended models often flexibilizes the adjustment of a model (say *baseline*) that has a connection more direct with the phenomenon origin, but it may not work well in practice. Further, the extensions include the baseline model as particular case, easily identified in the extended distribution parametric space. This last fact delivers to the future users of the proposal a simple rule (based on asymptotic results from maximum likelihood estimators) to choose between the baseline or extended models before actual scenarios.

*G. M. Cordeiro and A. D. C. Nascimento are with the Departamento de Estatística, Universidade Federal de Pernambuco (UFPE), Brazil. E-mail: gauss,abraao@de.ufpe.br

†R. J. Cintra is with the Signal Processing Group, CCEN, Universidade Federal de Pernambuco (UFPE), Brazil. E-mail: rjdc@de.ufpe.br

‡L. C. Rêgo is with the Departamento de Estatística e Matemática Aplicada, Universidade Federal do Ceará, Brazil. E-mail: leandro@dema.ufc.br

b) These extensions also may stem from a phenomenological justification and introduce baselines in a physical, industrial, and biological contexts:

- (i) Time to relapse of cancer under the first-activation scheme [5].
- (ii) The failure of a device which occurs due to the presence of an unknown number of factors [1, 19].
- (iii) Time of resistance to a disease manifestation due to the i th latent factor has the baseline distribution [31].

The generalized normal (“GN” for short) distribution with location parameter μ , dispersion parameter σ , and shape parameter s has probability density function (pdf) given by Nadarajah [23]

$$g(x) = \frac{s}{2\sigma \Gamma(1/s)} \exp\left\{-\left|\frac{x-\mu}{\sigma}\right|^s\right\}, \quad x \in \mathbb{R},$$

where $\Gamma(a) = \int_0^\infty t^{a-1} e^{-t} dt$ is the gamma function, μ is a real number, and σ and s are positive real numbers. For the special case $s = 1$, the above density function reduces to the Laplace distribution with location parameter μ and scale parameter σ . Similarly, for $s = 2$, the normal distribution is obtained with mean μ and variance $\sigma^2/2$. The main feature of the GN model is that the new parameter s can add some skewness and kurtosis.

The cumulative distribution function (cdf) of the GN distribution can be expressed as [23, Eq. 5-6]

$$G(x) = \begin{cases} \frac{\Gamma(1/s, (\frac{\mu-x}{\sigma})^s)}{2\Gamma(1/s)}, & x \leq \mu, \\ 1 - \frac{\Gamma(1/s, (\frac{x-\mu}{\sigma})^s)}{2\Gamma(1/s)}, & x > \mu, \end{cases} \quad (1)$$

where $\Gamma(s, x) = \int_x^\infty t^{s-1} e^{-t} dt$ is the upper incomplete gamma function.

The density function of the standardized random variable $Z = (X - \mu)/\sigma$ is

$$\phi_s(z) = \frac{s}{2\Gamma(1/s)} \exp(-|z|^s), \quad z \in \mathbb{R}.$$

Thus, $g(x) = \sigma^{-1} \phi_s(\frac{x-\mu}{\sigma})$. From Equation (1), the cdf of the standardized GN distribution reduces to

$$\Phi_s(z) = \begin{cases} \frac{\Gamma(1/s, (-z)^s)}{2\Gamma(1/s)}, & z \leq 0, \\ 1 - \frac{\Gamma(1/s, z^s)}{2\Gamma(1/s)}, & z > 0. \end{cases}$$

A family of univariate distributions generated by gamma random variables was pioneered by Zografos and Balakrishnan [35] and Ristić and N. Balakrishnan [28]. They defined the *gamma generalized-G* (“GG-G” for short) distribution from any baseline cdf $G(x)$, $x \in \mathbb{R}$, using an additional shape parameter $a > 0$. The associated pdf and cdf are given by

$$f(x) = \frac{g(x)}{\Gamma(a)} \{-\log[1 - G(x)]\}^{a-1} \quad (2)$$

and

$$F(x) = \frac{1}{\Gamma(a)} \int_0^{-\log[1-G(x)]} t^{a-1} e^{-t} dt = \gamma_1(a, -\log[1-G(x)]), \quad (3)$$

respectively, where $g(x) = dG(x)/dx$, $\gamma(a, z) = \int_0^z t^{a-1} e^{-t} dt$ is the lower incomplete gamma function and $\gamma_1(a, z) = \gamma(a, z)/\Gamma(a)$ is the lower incomplete gamma function ratio.

Each new GG-G distribution can be obtained from a specified G distribution. For $a = 1$, the G distribution is a basic exemplar with a continuous crossover towards cases with different shapes (for example, a particular combination of skewness and kurtosis). Zografos and Balakrishnan [35] motivated the GG distribution as follows. Let $X_{(1)}, \dots, X_{(n)}$ be lower record values from a sequence of independent and identically distributed (i.i.d.) random variables from a population with pdf $g(x)$. Then, the pdf of the n th lower record value is given by (2) with $a = n$. A logarithmic transformation of the baseline distribution G transforms the random variable X with density function (2) to a gamma distribution. In other words, if X has the density (2), then $Z = -\log[1 - G(X)] \sim \text{Gamma}(a, 1)$ has pdf expressed as

$$\pi(z; a) = \Gamma(a)^{-1} z^{a-1} e^{-z},$$

where $z \in \mathbb{R}_+$. The opposite is also true, if $Z \sim \text{Gamma}(a, 1)$, then the random variable $X = G^{-1}(1 - \exp[-Z])$ has the GG-G density function (2). Nadarajah *et al.* [24] derived some mathematical properties of (2) in the most simple, explicit, and general forms for any G distribution.

The first goal of this paper is to develop an extension of the generalized normal (GN) distribution defined from (2): the *gamma generalized normal* (“GGN” for short) distribution. It may be mentioned that although several skewed distributions exist on the positive real axis, not many skewed distributions are available on the whole real line, which are easy to use for data analysis purposes.

The main role of the extra parameter $a > 0$ is that the GGN distribution can be used to model skewed real data, a feature very common in practice. This distribution with four parameters can control location, dispersion, and skewness with great flexibility.

As a second goal, we advance the GGN distribution as a model for the image processing of SAR imagery [12]. We provide a data analysis using simulated and actual SAR imagery. Also, we compare the GGN model with the beta generalized normal (BGN) distribution introduced by Cintra *et al.* [6]. The BGN law has outperformed several existing models used for fitting SAR images, such as the gamma distribution [8], the \mathcal{K} distribution [3], and the \mathcal{G}^0 distribution [14]. The gamma distribution is regarded as standard model for the herein considered types of SAR data [8]. For such, actual data is analyzed and fitted according to GGN and BGN models above by means of eight figures of merit [15]. The model we propose outperforms the BGN distribution. In particular, the BGN has failed to describe regions having more than one texture for all considered channels, the GGN works well.

The rest of the paper is organized as follows. In Section 2, we define the GGN distribution, derive its density, discuss special cases and provide some of its characteristics. A useful expansion for its density function is determined in Section 3. Explicit expressions for the moments are derived in Section 4. Maximum likelihood estimation of the model parameters is investigated in Section 5. In Section 6, we propose a random number generator for the new distribution. Section 7 details the SAR image analysis based on real data. Section 8 provides concluding remarks.

2 The GGN Distribution

Based on Equations (2) and (3), we propose a generalization of the GN distribution and provide a comprehensive treatment of its mathematical properties. The pdf and cdf of the GGN distribution are given by

$$f(x) = \frac{\phi_s\left(\frac{x-\mu}{\sigma}\right)}{\sigma\Gamma(a)} \left\{ -\log\left[1 - \Phi_s\left(\frac{x-\mu}{\sigma}\right)\right] \right\}^{a-1} \quad (4)$$

and

$$F(x) = \frac{1}{\Gamma(a)} \int_0^{-\log[1-\Phi_s(\frac{x-\mu}{\sigma})]} t^{a-1} e^{-t} dt = \gamma_1\left(a, -\log\left[1 - \Phi_s\left(\frac{x-\mu}{\sigma}\right)\right]\right).$$

Here, the parameter a affects the skewness through the relative tail weights. It provides greater flexibility in the form of the distribution and consequently in modeling observed real data. Hereafter, a random variable X with density function (4) is denoted by $X \sim \text{GGN}(\mu, \sigma, s, a)$. Notice that the gamma normal and gamma Laplace distributions are special cases of (4) for $s = 1$ and $s = 2$, respectively. The baseline GN distribution is also a sub-model for $a = 1$. The normal distribution arises for $a = 1$ and $s = 2$, whereas the Laplace distribution corresponds to $a = s = 1$. A noteworthy property of (4) is its ability for fitting skewed real data that cannot be properly fitted by existing distributions with support on the real line. Location and scale parameters can be set to zero and one, respectively, in (4). This is because if $W \sim \text{GGN}(0, 1, s, a)$ then $X = \sigma W + \mu \sim \text{GGN}(\mu, \sigma, s, a)$.

The GGN distribution has two important interpretations. First, given a sequence of independent and identically GN random variables with cdf (1), the GGN density function coincides with the density function of the a th lower record value if a is a positive integer. As a consequence, (4) can be considered as a generalization of the density function of GN lower records. Record values arise naturally in many real life problems relating to engineering, economics and medicine. Secondly, if Z has a gamma density with scale parameter one and shape parameter a , the GN quantile function evaluated at the random variable $1 - e^{-z}$ has pdf given by (4).

Note that the limiting behavior of the GN density with respect to s is given by

$$\lim_{s \rightarrow \infty} \phi_s(z) = \lim_{s \rightarrow \infty} \frac{s}{2\Gamma(1/s)} \exp(-|z|^s) = \begin{cases} \frac{1}{2}, & |z| < 1, \\ 0, & \text{otherwise.} \end{cases}$$

Consequently, by invoking the dominate convergence theorem, we obtain:

$$\lim_{s \rightarrow \infty} \Phi_s(z) = \begin{cases} 0, & z < -1, \\ \frac{1}{2}(z+1), & |z| < 1, \\ 1, & z > 1. \end{cases}$$

Making appropriate substitutions, the limiting distribution $\lim_{s \rightarrow \infty} f(x)$ is given by

$$\begin{aligned} \lim_{s \rightarrow \infty} f(x) &= \frac{1}{2\sigma\Gamma(a)} \left\{ -\log\left[1 - \left(\frac{1}{2} + \frac{x-\mu}{2\sigma}\right)\right] \right\}^{a-1} \\ &= f_{\text{GU}}\left(\frac{x-\mu}{\sigma}\right), \quad x \in [\mu - \sigma, \mu + \sigma], \end{aligned}$$

where $f_{\text{GU}}(x)$ is the pdf of the gamma uniform random variable associated to the uniform distribution over the

interval $[-1, 1]$. Figure 1 illustrates this behavior.

3 Density expansion

Expansions for (2) and (3) can be derived using the concept of exponentiated distributions. Consider the *exponentiated generalized normal* (“EGN”) distribution with power parameter $c > 0$ defined by $Y_c \sim \text{EGN}(\mu, \sigma, s, c)$ having cdf and pdf given by

$$H_c(x) = \begin{cases} \left[\frac{\Gamma(1/s, (\frac{\mu-x}{\sigma})^s)}{2\Gamma(1/s)} \right]^c, & x \leq \mu, \\ \left[1 - \frac{\Gamma(1/s, (\frac{x-\mu}{\sigma})^s)}{2\Gamma(1/s)} \right]^c, & x > \mu, \end{cases} \quad (5)$$

and

$$h_c(x) = \begin{cases} \frac{s}{2\sigma\Gamma(1/s)} \exp\left\{-\left|\frac{x-\mu}{\sigma}\right|^s\right\} \left[\frac{\Gamma(1/s, (\frac{\mu-x}{\sigma})^s)}{2\Gamma(1/s)} \right]^{c-1}, & x \leq \mu, \\ \frac{s}{2\sigma\Gamma(1/s)} \exp\left\{-\left|\frac{x-\mu}{\sigma}\right|^s\right\} \left[1 - \frac{\Gamma(1/s, (\frac{x-\mu}{\sigma})^s)}{2\Gamma(1/s)} \right]^{c-1}, & x > \mu, \end{cases} \quad (6)$$

respectively. The properties of some exponentiated distributions have been studied by several authors, see Mudholkar and Srivastava [21], Mudholkar *et al.* [22] for the exponentiated Weibull (EW), Gupta *et al.* [17] for the exponentiated Pareto, Gupta and Kundu [18] for the exponentiated exponential (EE), Nadarajah and Gupta [25] for exponentiated gamma (EG) distributions, and Cordeiro *et al.* [7] for the exponentiated generalized gamma (EGG) distribution.

Based on an expansion due to Nadarajah *et al.* [24], we can write

$$\begin{aligned} \left\{ -\log \left[1 - \Phi_s \left(\frac{y-\mu}{\sigma} \right) \right] \right\}^{a-1} &= (a-1) \sum_{k=0}^{\infty} \binom{k+1-a}{k} \sum_{j=0}^k \frac{(-1)^{j+k} \binom{k}{j} p_{j,k}}{(a-1-j)} \\ &\quad \times \Phi_s \left(\frac{y-\mu}{\sigma} \right)^{a+k-1}, \end{aligned}$$

where $a > 0$ is any real parameter and the constants $p_{j,k}$ can be calculated recursively by

$$p_{j,k} = k^{-1} \sum_{m=1}^k \frac{(-1)^m [m(j+1) - k]}{(m+1)} p_{j,k-m},$$

for $k = 1, 2, \dots$ and $p_{j,0} = 1$. Let

$$b_k = \frac{\binom{k+1-a}{k}}{(a+k)\Gamma(a-1)} \sum_{j=0}^k \frac{(-1)^{j+k} \binom{k}{j} p_{j,k}}{(a-1-j)}.$$

Then, (4) can be expressed as

$$f(x) = \sum_{k=0}^{\infty} b_k h_{a+k}(x), \quad (7)$$

where $h_{a+k}(x)$ denotes the density function of the random variable $Y_{a+k} \sim \text{EGN}(a+k, \mu, \sigma, s)$ given by (6). The

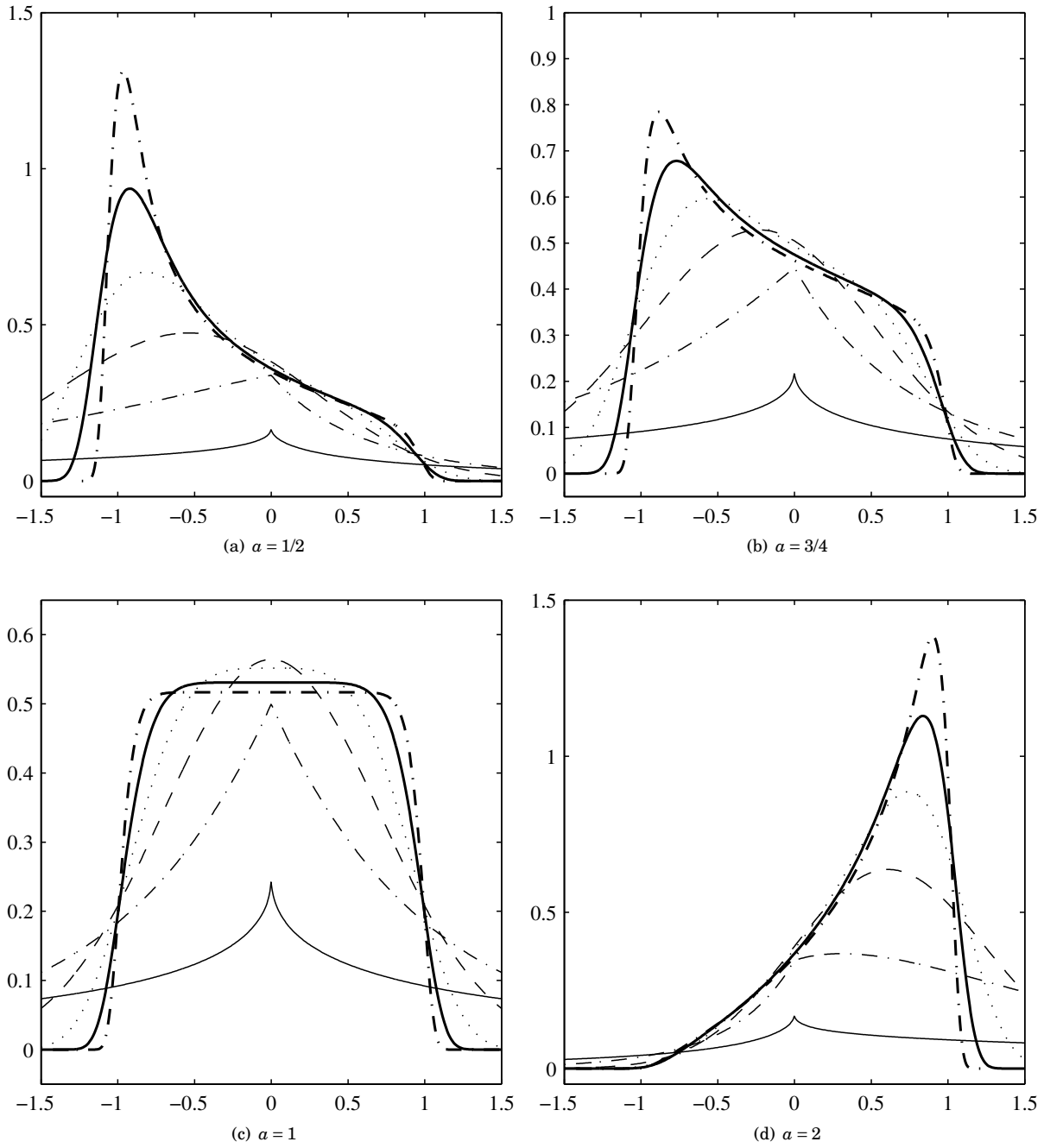


Figure 1: Plots of the GGN density function for some parameter values: $\mu = 0$, $\sigma = 1$, and $s \in \{16, 8, 4, 2, 1, 1/2\}$ (dash-dotted, solid, dotted, dashed, dash-dotted, solid).

cdf corresponding to (7) becomes

$$F(x) = \sum_{k=0}^{\infty} b_k H_{a+k}(x), \quad (8)$$

where $H_{a+k}(x)$ denotes the cumulative function of Y_{a+k} given by (5).

4 Moments

Let X be a random variable having the GGN(μ, σ, s, a) distribution. The n th moment of X becomes

$$\mathbb{E}(X^n) = \sum_{k=0}^{\infty} \frac{(a+k)b_k}{\sigma} \int_{-\infty}^{\infty} x^n \left[\Phi_s\left(\frac{x-\mu}{\sigma}\right) \right]^{a+k-1} \phi_s\left(\frac{x-\mu}{\sigma}\right) dx. \quad (9)$$

Defining the auxiliary function $h_k^{(s)}(x) = \Phi_s\left(\frac{x-\mu}{\sigma}\right)^{a+k-1} \phi_s\left(\frac{x-\mu}{\sigma}\right)$ and setting $z = \frac{x-\mu}{\sigma}$, we can write

$$\begin{aligned} \int_{-\infty}^{\infty} x^n h_k^{(s)}(x) dx &= \sigma \int_{-\infty}^{\infty} (\sigma z + \mu)^n \Phi_s(z)^{a+k-1} \phi_s(z) dz \\ &= \sigma \mu^n \sum_{i=0}^n \binom{n}{i} \left(\frac{\sigma}{\mu}\right)^i \int_{-\infty}^{\infty} z^i \Phi_s(z)^{a+k-1} \phi_s(z) dz. \end{aligned} \quad (10)$$

Splitting the integration range in (10) in two parts and considering that $\Phi_s(-z) = 1 - \Phi_s(z)$ and $\phi_s(z) = \phi_s(-z)$, we have

$$\begin{aligned} \int_{-\infty}^{\infty} z^i \phi_s(z) \Phi_s(z)^{a+k-1} dz &= \int_0^{\infty} z^i \phi_s(z) \Phi_s(z)^{a+k-1} dz \\ &\quad + \int_0^{\infty} (-1)^i z^i \phi_s(z) [1 - \Phi_s(z)]^{a+k-1} dz. \end{aligned}$$

We can express $\Phi_s(z)^\alpha$ for any real $\alpha > 0$ in terms of a power series of $\Phi_s(z)$, namely $\Phi_s(z)^\alpha = \sum_{j=0}^{\infty} v_j(\alpha) \Phi_s(z)^j$, where $v_j(\alpha) = \sum_{m=j}^{\infty} (-1)^{j+m} \binom{\alpha}{m} \binom{m}{j}$. Thus, based on this expansion, we obtain

$$\begin{aligned} \int_{-\infty}^{\infty} z^i \phi_s(z) \Phi_s(z)^{a+k-1} dz &= \\ \sum_{j=0}^{\infty} v_j(a+k-1) \int_0^{\infty} z^i \phi_s(z) \Phi_s(z)^j dz & \\ + \sum_{j=0}^{\infty} (-1)^{i+j} \binom{a+k-1}{j} \int_0^{\infty} z^i \phi_s(z) \Phi_s(z)^j dz. & \end{aligned}$$

We define the (i, j) th probability weighted moment of Z by $J_{i,j}^{(s)} = \int_0^{\infty} z^i \phi_s(z) \Phi_s(z)^j dz$, where i, j are positive integers. Cintra *et al.* [6] demonstrated that

$$\begin{aligned} J_{i,j}^{(s)} &= \frac{1}{[2\Gamma(1/s)]^{j+1}} \sum_{r=0}^j \binom{j}{r} \Gamma(s^{-1})^{j-r} \\ &\quad \times \sum_{m=0}^{\infty} c_{m,r} \Gamma\left(m + \frac{i+r+1}{s}\right), \end{aligned} \quad (11)$$

where $c_{0,r} = s^r$ and for all $m \geq 1$

$$c_{m,r} = (ms)^{-1} \sum_{\ell=1}^m \frac{(-1)^\ell [(r+1)\ell - m]}{(s^{-1} + \ell)\ell!} c_{m-\ell,r}.$$

Hence, we obtain:

$$\begin{aligned} & \int_{-\infty}^{\infty} z^i \phi_s(z) \Phi_s(z)^{a+k-1} dz = \\ & \sum_{j=0}^{\infty} \left[v_j (a+k-1) + (-1)^{i+j} \binom{a+k-1}{j} \right] \mathcal{J}_{i,j}^{(s)}. \end{aligned} \quad (12)$$

Finally, based on (9), (10) and (12), we have the following expression:

$$\begin{aligned} \mathbb{E}(X^n) &= \sum_{k,j=0}^{\infty} (a+k) b_k \sum_{i=0}^n \binom{n}{i} \frac{\sigma}{\mu^{i-n}} \\ & \times \left[v_j (a+k-1) + (-1)^{i+j} \binom{a+k-1}{j} \right] \mathcal{J}_{i,j}^{(s)}. \end{aligned} \quad (13)$$

The above expression is the main result of this section.

5 Maximum Likelihood Estimation

Consider a random variable X having the GGN distribution and let $\theta = (\mu, \sigma, s, a)^\top$ be the model parameters. Thus, the associated log-likelihood function for one observation x is

$$\begin{aligned} \ell(\theta) = \ell(\theta; x) &= \log \left[\phi_s \left(\frac{x-\mu}{\sigma} \right) \right] - \log(\sigma) - \log[\Gamma(a)] \\ & + (a-1) \log \left\{ -\log \left[1 - \Phi_s \left(\frac{x-\mu}{\sigma} \right) \right] \right\}. \end{aligned} \quad (14)$$

The maximum likelihood estimate (MLE) of θ is determined by maximizing $\ell_n(\theta) = \sum_{i=1}^n \ell(\theta; x_i)$ from a dataset x_1, x_2, \dots, x_n .

Based on Equation (14), the score function can be derived as follows

$$\begin{aligned} U_\theta &= (U_\mu, U_\sigma, U_s, U_a)^\top \\ &= \left(\frac{d\ell(\theta)}{d\mu}, \frac{d\ell(\theta)}{d\sigma}, \frac{d\ell(\theta)}{ds}, \frac{d\ell(\theta)}{da} \right)^\top. \end{aligned}$$

To that end, we consider initially the discussion of some auxiliary results. After some algebra, two identities hold:

$$\frac{d\Phi_s \left(\frac{x-\mu}{\sigma} \right)}{d\delta} = C_\delta \phi_s \left(\frac{x-\mu}{\sigma} \right) \quad (15)$$

and

$$\frac{d \log \phi_s \left(\frac{x-\mu}{\sigma} \right)}{d\delta} = -s C_\delta \operatorname{sign}(x-\mu) \left| \frac{x-\mu}{\sigma} \right|^{s-1}, \quad (16)$$

where $\delta \in \{\mu, \sigma\}$, $C_\mu = -\sigma^{-1}$ and $C_\sigma = \mu/\sigma^2$. Another result required for the subsequent derivations is $\frac{d}{ds}\Phi_s\left(\frac{x-\mu}{\sigma}\right)$, which depends on the derivatives of the gamma and the incomplete gamma functions. Cintra *et al.* [6] demonstrated that identities (15) and (16) for $\delta = s$ are given by

$$\frac{d\Phi_s\left(\frac{x-\mu}{\sigma}\right)}{ds} = \frac{1}{2\Gamma(1/s)} \times \begin{cases} s^2 \tilde{\psi}\left(s, \left(\frac{\mu-x}{\sigma}\right)^s\right) + \psi(1/s)\Gamma(1/s, \left(\frac{\mu-x}{\sigma}\right)^s), & x \leq \mu, \\ -[s^2 \tilde{\psi}\left(s, \left(\frac{x-\mu}{\sigma}\right)^s\right) + \psi(1/s)\Gamma(1/s, \left(\frac{x-\mu}{\sigma}\right)^s)], & x > \mu, \end{cases}$$

where $\psi(x)$ is the digamma function, and $\tilde{\psi}(s, x) \triangleq \frac{d\Gamma(1/s, x^s)}{ds}$, for $x > 0$ [6]. Additionally, the following result was also presented by Cintra *et al.*:

$$\frac{d \log \phi_s\left(\frac{x-\mu}{\sigma}\right)}{ds} = \frac{1}{s} + \frac{\psi(1/s)}{s^2} - \left|\frac{x-\mu}{\sigma}\right|^s \log\left(\left|\frac{x-\mu}{\sigma}\right|\right).$$

The elements of the GGN score function are given in Fig. 2.

$$U_\mu = \frac{s}{\sigma} \text{sign}(x - \mu) \left|\frac{x - \mu}{\sigma}\right|^{s-1} - \left(\frac{a-1}{\sigma}\right) \frac{\phi_s\left(\frac{x-\mu}{\sigma}\right)}{[1 - \Phi_s\left(\frac{x-\mu}{\sigma}\right)] \log[1 - \Phi_s\left(\frac{x-\mu}{\sigma}\right)]}, \quad (17)$$

$$U_\sigma = -\frac{s\mu}{\sigma^2} \text{sign}(x - \mu) \left|\frac{x - \mu}{\sigma}\right|^{s-1} - \frac{1}{\sigma} + \left[\frac{(a-1)\mu}{\sigma^2}\right] \frac{\phi_s\left(\frac{x-\mu}{\sigma}\right)}{[1 - \Phi_s\left(\frac{x-\mu}{\sigma}\right)] \log[1 - \Phi_s\left(\frac{x-\mu}{\sigma}\right)]}, \quad (18)$$

$$U_s = \frac{d \log \phi_s\left(\frac{x-\mu}{\sigma}\right)}{ds} + (a-1) \frac{\frac{d\Phi_s\left(\frac{x-\mu}{\sigma}\right)}{ds}}{[1 - \Phi_s\left(\frac{x-\mu}{\sigma}\right)] \log[1 - \Phi_s\left(\frac{x-\mu}{\sigma}\right)]} \quad (19)$$

$$U_a = \log\left\{-\log\left[1 - \Phi_s\left(\frac{x-\mu}{\sigma}\right)\right]\right\} - \psi(a). \quad (20)$$

Figure 2: The GGN score function.

6 GGN Random Number Generator

Here, we give a random number generator (RNG) for the proposed distribution. This RNG provides a Monte Carlo study to determine the influence of the GGN shape parameters s and a .

Among the algorithms for generating continuous random variables, we use the inverse transform due to its analytical tractability [29, p. 67]. Let $X \sim \text{GGN}(\mu, \sigma, s, a)$. Then, as discussed in Section 1, X can be associated with $Z \sim \text{Gamma}(a, 1)$ according to the identity:

$$X = G^{-1}(1 - e^{-Z}).$$

Notice that

$$G(x) = \begin{cases} \frac{1}{2} \{1 - F_{\Gamma} [(-\frac{x-\mu}{\sigma})^s]\}, & x \leq \mu, \\ \frac{1}{2} \{1 + F_{\Gamma} [(\frac{x-\mu}{\sigma})^s]\}, & x > \mu, \end{cases}$$

where $F_{\Gamma}(\cdot)$ is the gamma cdf with shape and scale parameters given by $1/s$ and one, respectively.

Let x and z be realizations of X and Z , respectively. For $x \leq \mu$, we obtain the inverse transformation according to the following equation

$$\frac{1}{2} \{1 - F_{\Gamma} [(-\frac{x-\mu}{\sigma})^s]\} = 1 - e^{-z}.$$

Therefore,

$$x = \mu - \sigma [F_{\Gamma}^{-1}(2e^{-z} - 1)]^{1/s},$$

where $F_{\Gamma}^{-1}(\cdot)$ is the quantile function of the gamma distribution with parameters $1/s$ and one. Since $0 \leq F_{\Gamma} [(-\frac{x-\mu}{\sigma})^s] \leq 1$, we have $0 \leq z \leq \log 2$.

Analogously, for $x > \mu$, we obtain:

$$x = \mu + \sigma [F_{\Gamma}^{-1}(1 - 2e^{-z})]^{1/s}, \quad \log 2 < z < \infty.$$

Thus, the generation of X can follow the algorithm:

- 1: Generate $Z \sim \Gamma(a, 1)$
- 2: **if** $Z \in [0, \log 2]$ **then**
- 3: $X = \mu - \sigma [F_{\Gamma}^{-1}(2e^{-Z} - 1)]^{1/s}$
- 4: **else**
- 5: $X = \mu + \sigma [F_{\Gamma}^{-1}(1 - 2e^{-Z})]^{1/s}$
- 6: **return** X .

Figure 3 provides six cases clustered on two graphics where theoretical curves are compared with randomly generated points. The GGN law at $\theta = (0, 1, s, 5)^{\top}$ such that $s \in \{0.6, 0.8, 1.0\}$ is considered in Figure 3(a). Data and density curves from $X \sim \text{GGN}(0, 1, 0.5, a)$ such that $a \in \{1, 1.5, 4\}$ are displayed in Figure 3(b).

7 SAR Image Processing

In this section, we assess the GGN model performance on both synthetic and actual data. Using Monte Carlo experiments, we first employ the proposed GGN RNG method to generate synthetic data in order to quantify the influence of shape parameters a and s on the asymptotic properties of the MLEs. Subsequently, we apply the GGN model to actual SAR data, which require a specialized model due to the presence of the speckled noise in SAR imagery.

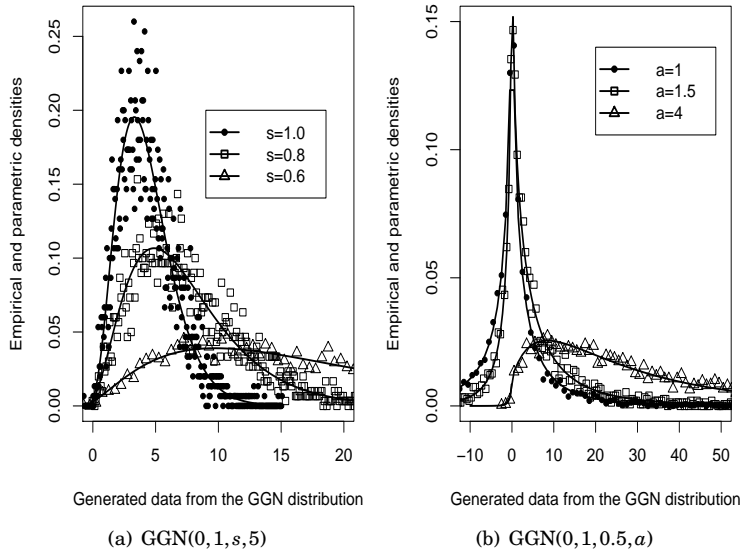


Figure 3: GGN random number generation.

7.1 Parameter study

In order to quantify the influence of the shape parameters (a and s) on the MLEs from the proposed distribution and on their corresponding mean square errors (MSEs), we perform $M = 5500$ Monte Carlo replications. This simulation study follows the scheme:

1. Synthetic data were generated from the GGN distribution, simulating images of 5×5 , 7×7 , and 11×11 pixels. Therefore, we have samples sizes of $N \in \{25, 49, 121\}$.
2. By fixing the parameters $\mu = 0$ and $\sigma = 1$, nine scenarios are considered for $a \in \{2, 3\}$ and $s \in \{1, 2, 3\}$.
3. As assessing criteria, the average of the MLEs and their corresponding estimates for the MSEs are computed.

Table 1 presents the numerical values for the selected criteria. In general terms, as expected, the results indicate that increasing the sample sizes decreases the MSE and the estimates become closer to the true parameters in average. In addition, the estimates for s assume the worse values among them; i.e., the estimates of the MSE corresponding to s converge more slowly to zero.

7.2 SAR Image Modeling

Polarimetric SAR (PolSAR) devices have been considered one of most important tools for sensing geophysical scenarios [20]. Such systems work under the following dynamic: orthogonally polarized pulses (in vertical, 'V', or horizontal, 'H', directions) are transmitted towards a target, and the returned echoes are recorded with respect to each polarization. Resulting images can be understood as outcomes from a sequence either (i) of complex random vectors (called *single look*) or (ii) of Hermitian positive definite random matrices (called

Table 1: Average of the estimated parameters and their respective estimates for the mean square errors

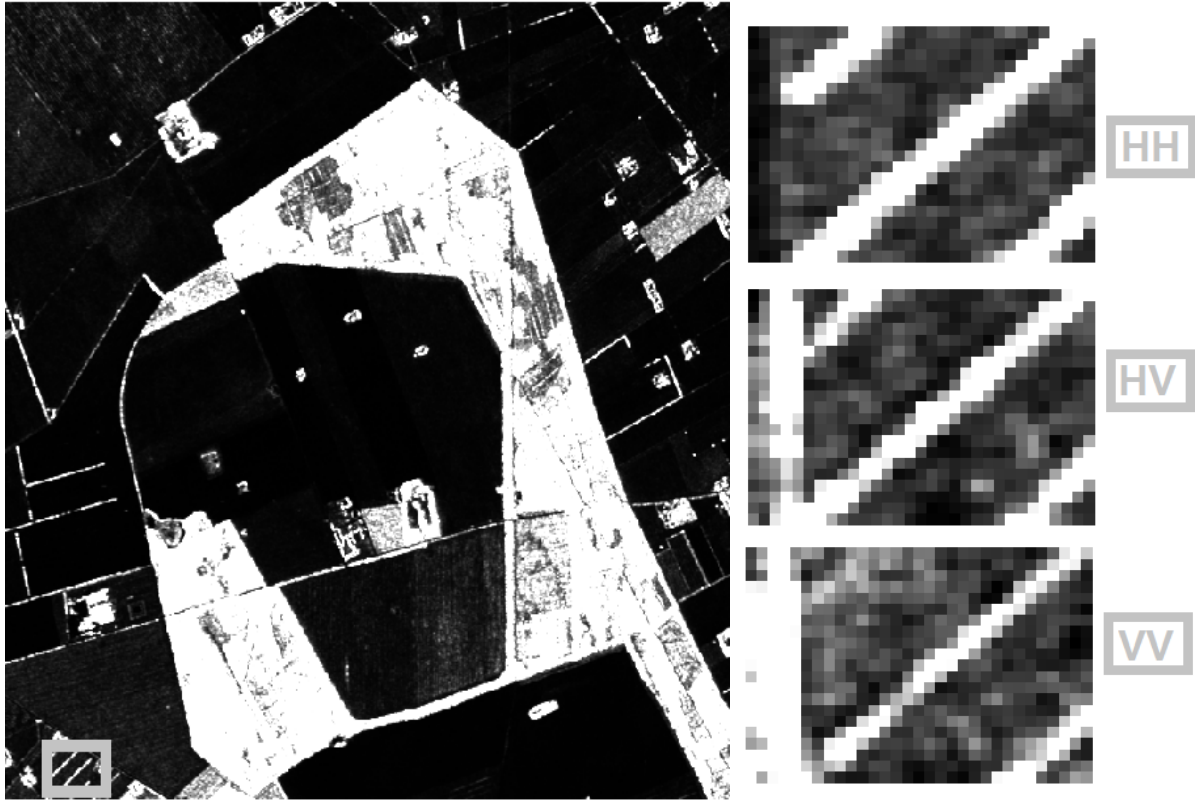
N	<i>Estimated parameters (MSE)</i>			
$(a, \mu, \sigma, s) = (2, 0, 1, 1)$				
25	2.305(0.668)	-0.0418(0.264)	0.760(0.368)	1.251(8.203)
49	2.203(0.416)	-0.0498(0.165)	0.861(0.176)	0.981(0.128)
121	2.097(0.160)	-0.0318(0.063)	0.944(0.066)	0.991(0.024)
$(a, \mu, \sigma, s) = (2, 0, 1, 2)$				
25	2.179(0.995)	0.032(0.220)	0.886(0.164)	6.294(121.926)
49	2.248(1.146)	-0.024(0.253)	0.943(0.093)	2.907(13.092)
121	2.254(1.151)	-0.049(0.267)	0.967(0.044)	2.119(0.460)
$(a, \mu, \sigma, s) = (2, 0, 1, 3)$				
25	1.818(0.706)	0.143(0.167)	0.943(0.064)	10.673(211.943)
49	1.921(0.639)	0.074(0.147)	0.988(0.036)	5.232(33.199)
121	2.022(0.499)	0.007(0.111)	1.011(0.019)	3.416(1.040)
$(a, \mu, \sigma, s) = (3, 0, 1, 1)$				
25	3.402(0.675)	0.037(0.290)	0.742(0.474)	1.151(5.995)
49	3.241(0.426)	-0.005(0.152)	0.840(0.221)	0.953(0.098)
121	3.148(0.274)	-0.010(0.078)	0.901(0.097)	0.966(0.021)
$(a, \mu, \sigma, s) = (3, 0, 1, 2)$				
25	2.886(1.279)	0.224(0.261)	0.824(0.164)	4.522(62.262)
49	2.956(1.246)	0.142(0.236)	0.903(0.093)	2.573(7.336)
121	3.002(1.157)	0.073(0.219)	0.958(0.043)	2.096(0.369)
$(a, \mu, \sigma, s) = (3, 0, 1, 3)$				
25	2.471(1.401)	0.303(0.256)	0.833(0.124)	7.228(93.527)
49	2.553(1.177)	0.228(0.210)	0.904(0.067)	4.235(16.030)
121	2.710(0.921)	0.134(0.157)	0.957(0.037)	3.228(0.564)

multilook) [2]. Here, we address the multilook case, considering the proposal of statistical models for elements of the main diagonal of resulting matrices from PolSAR images.

Figure 4(a) presents an image over the surroundings of Foulum (Denmark) obtained by the EMISAR system [9]. This is a polarimetric SAR image, i.e., each of its pixels is represented by a particular 3×3 Hermitian positive definite matrices, whose diagonal elements are positive real intensities:

$$Z = \begin{bmatrix} |Z_{HH}| & Z_{HH-HV} & Z_{HH-VV} \\ Z_{HH-HV}^* & |Z_{HV}| & Z_{HV-VV} \\ Z_{HH-VV}^* & Z_{HV-VV}^* & |Z_{VV}| \end{bmatrix},$$

where $\{|Z_{HH}|, |Z_{HV}|, |Z_{VV}|\}$ represents the set of intensities from Z_{HH} , Z_{HV} , and Z_{VV} polarization channels (complex random vectors) and $\{Z_{HH-HV}, Z_{HH-VV}, Z_{HV-VV}\}$ indicates the set of possible products between two different polarization channels such that $Z_{A-B} = Z_A Z_B^*$, for $A, B \in \{HH, HV, VV\}$, and $*$ denotes the conjugate of a complex number. The intensities of the echoed signal polarization channels play an important role, since they depend on the physical properties of the target surface. We aim to show that the proposed model is an adequate representation for the a pre-processing step in SAR image processing due to one channel. Figure 4(b) illustrates the images of the corresponding polarization channels.



(a) Total image

(b) HV, VV, and HH region images

Figure 4: SAR image with the selected region and images of data of HH, HV, and VV associated polarization channels.

Figure 5 gives empirical and fitted densities on EMISAR real data. The GGN model is compared with the BGN distribution [6]. Such distribution outperforms classical models for intensity SAR data, such as \mathcal{G}_I^0 , \mathcal{K} , and Γ distributions; however, it has five parameters which usually offers computational difficulties, because the MLEs are defined as the solution of a system with five nonlinear equations. The fitted empirical density plots shown in Figures 5(a)-5(c) suggest the appropriateness of the GGN model. In comparison with the BGN, Γ , and beta distributions, the GGN model offers better fitted empirical densities. Table 2 presents the corresponding MLEs and their respective estimates for the mean square errors for the parameters of GGN, BGN, Γ , and beta distributions on data from each polarization channel.

Table 2: ML estimates for the BGN($s, \mu, \sigma, \alpha, \beta$) [6], GGN(a, μ, σ, s), $\Gamma(\alpha, \beta)$ and beta(α, β) distributions. Standard errors are in parenthesis.

Model	Estimated Parameters				
<i>For the HH channel</i>					
BGN	0.995 (0.128)	2.448×10^{-2} (0.312×10^{-2})	1.972×10^{-2} (0.429×10^{-2})	1.498 (0.585)	0.407 (0.098)
GGN	1.803 (0.192)	3.031×10^{-2} (1.950×10^{-3})	8.232×10^{-4} (8.834×10^{-5})	0.356 (5.707×10^{-3})	•
Γ	1.517 (0.086)	19.946 (1.399)	•	•	•
beta	0.607 (0.044)	7.372 (0.663)	•	•	•
<i>For the HV channel</i>					
BGN	0.989 (0.122)	3.603×10^{-3} (0.644×10^{-3})	2.595×10^{-3} (0.318×10^{-3})	0.949 (0.571)	0.232 (0.212)
GGN	1.821 (0.113)	3.965×10^{-3} (2.602×10^{-4})	5.031×10^{-5} (9.410×10^{-6})	3.084×10^{-1} (8.373×10^{-3})	•
Γ	1.045 (0.034)	79.817 (1.605)	•	•	•
beta	0.528 (0.017)	39.835 (1.638)	•	•	•
<i>For the VV channel</i>					
BGN	0.634 (0.099)	2.499×10^{-2} (0.212×10^{-2})	2.107×10^{-3} (1.429×10^{-3})	1.243 (0.881)	0.285 (0.120)
GGN	1.955 (7.089×10^{-2})	2.592×10^{-2} (4.965×10^{-4})	1.369×10^{-3} (3.347×10^{-5})	0.433420 (4.771×10^{-3})	•
Γ	2.67 (8.578×10^{-2})	52.590 (1.546)	•	•	•
beta	1.436 (9.029×10^{-2})	26.848 (2.027)	•	•	•

In order to compare the BGN and GGN models for the current data, we consider two discrimination measures based on information-theoretical tools [11, 32]. Let X be a random variable with density $f_X(x)$ and P_n the empirical density obtained from a data set. The following sample goodness-of-fits measures are considered:

- a) Symmetrized Kullback-Leibler divergence [11, 30]:

$$\begin{aligned}
 d_{\text{KL}}(X) &\equiv d_{\text{KL}}(X, P_n) \\
 &= \sum_{i=1}^N \left\{ f_X(X_i; \hat{\theta}_x) \log \left[\frac{f_X(X_i; \hat{\theta}_x)}{P_i} \right] \right. \\
 &\quad \left. + P_i \log \left[\frac{P_i}{f_X(X_i; \hat{\theta}_x)} \right] \right\}
 \end{aligned}$$

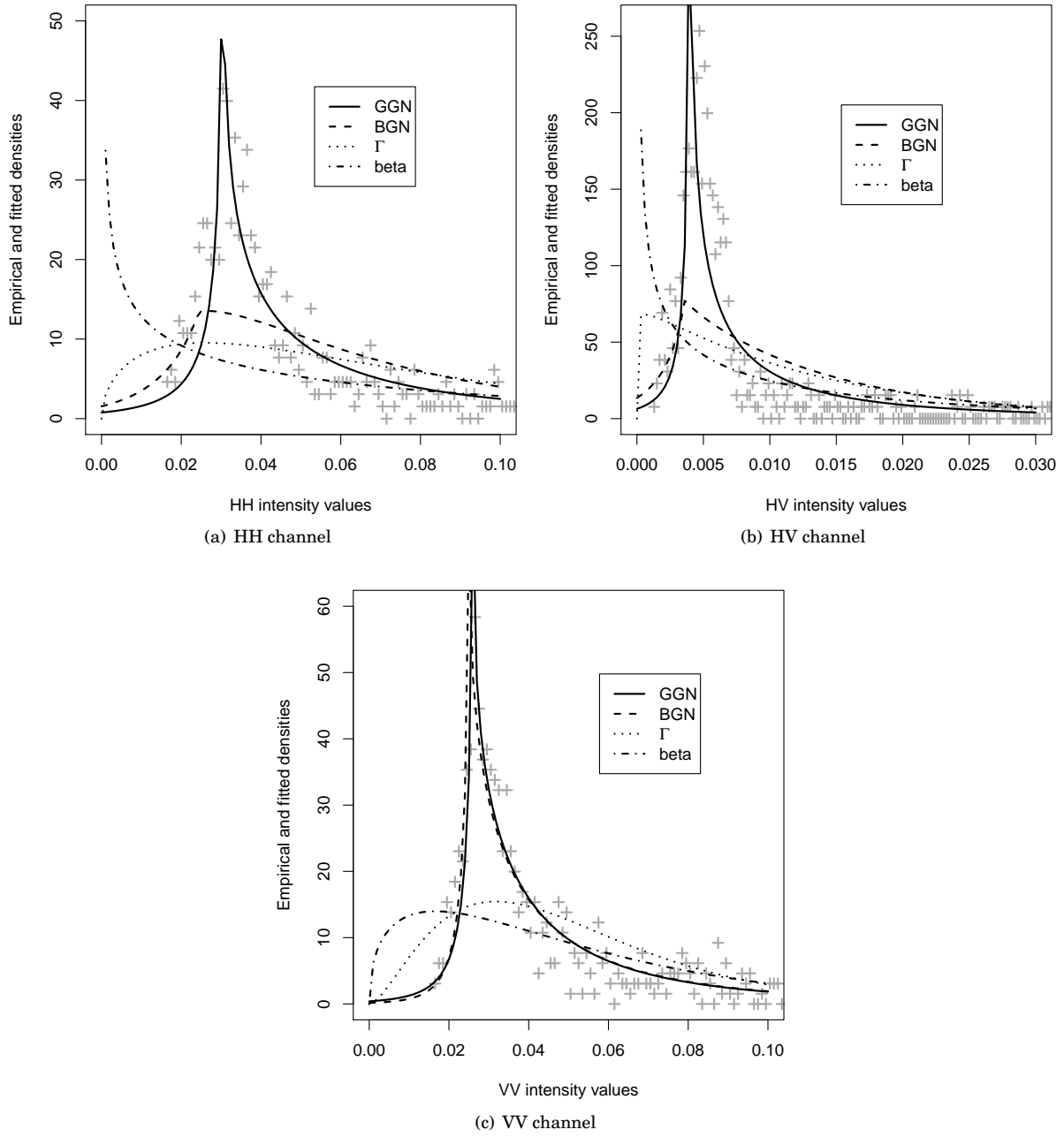


Figure 5: Empirical densities of the channel data.

Table 3: Goodness-of-fit measures for the fitted BGN, GGN, Γ and beta distributions on EMISAR real data

Goodness-of-fit measures	Channel	Performance for different model			
		GGN	BGN	Γ	beta
$d_{\text{KL}}(X)$	HH	37.957	104.992	126.852	121.491
$d_{\chi^2}(X)$		107.403	223.218×10^2	578.139×10	701.5747
d_{KS}		0.053	0.163	0.196	0.304
W^*		0.452	5.396	7.392	8.116
A^*		3.450	29.159	39.597	43.120
AIC		-2.495×10^3	-2.225×10^3	-2.108×10^3	-1.844×10^3
AIC_c		-2.493×10^3	-2.223×10^3	-2.106×10^3	-1.842×10^3
BIC		-2.490×10^3	-2.222×10^3	-2.099×10^3	-1.835×10^3
$d_{\text{KL}}(X)$	HV	371.397	898.627	962.826	849.346
$d_{\chi^2}(X)$		912.831	297.285×10	285.695×10	225.040×10
d_{KS}		0.117	0.302	0.275	0.276
W^*		1.563	9.112	11.219	11.246
A^*		9.002	47.860	58.162	58.241
AIC		-4.777×10^3	-4.428×10^3	-4.340×10^3	-4.177×10^3
AIC_c		-4.775×10^3	-4.426×10^3	-4.338×10^3	-4.175×10^3
BIC		-4.772×10^3	-4.425×10^3	-4.331×10^3	-4.168×10^3
$d_{\text{KL}}(X)$	VV	78.428	98.590	272.411	247.027
$d_{\chi^2}(X)$		211.659	261.400	978.570×10	102.669×10
d_{KS}		0.049	5.125×10^{-2}	0.174	0.216
W^*		0.262	0.247	5.945	6.238
A^*		1.900	1.514	32.422	33.924
AIC		-3.191×10^3	-3.200×10^3	-2.847×10^3	-2.728×10^3
AIC_c		-3.189×10^3	-3.198×10^3	-2.845×10^3	-2.726×10^3
BIC		-3.186×10^3	-3.197×10^3	-2.838×10^3	-2.719×10^3

b) Symmetrized chi-square divergence [32]:

$$d_{\chi^2}(X) \equiv d_{\chi^2}(X, P_n) = \sum_{i=1}^N \left[\frac{(f_X(X_i; \hat{\theta}_x) - P_i)^2}{f_X(X_i; \hat{\theta}_x)} + \frac{(f_X(X_i; \hat{\theta}_x) - P_i)^2}{P_i} \right].$$

Additionally, we also use the classical Kolmogorov–Smirnov (d_{KS}), Anderson–Darling (A^*) and Crámer–von Mises (W^*) statistics [13]. These measures are more adequate than the Akaike information criterion (AIC), corrected AIC (AIC_c), and Bayesian information criterion (BIC) measures. The latter ones are more recommended for nested models [33]. Table 3 presents the values of these eight measures for comparing the GGN and BGN models in terms of their distributions from intensity SAR data.

In general, comparisons favor the GGN model. An exception to this behavior is the group of measures $\{\text{AIC}, \text{AIC}_c, \text{BIC}\}$ for the VV channel. In this case, the BGN distribution is the best descriptor of SAR VV channel intensities. However, according to Voung [33], the group $\{\text{AIC}, \text{AIC}_c, \text{BIC}\}$ is more suitable for nested models, which is not the case in the GGN, BGN, Γ , and beta models. As a consequence, we suggest the GGN model as a meaningful model to describe SAR data from HH and VV channels.

7.3 AIRSAR Sensor Imagery Analysis

In this section, we apply the proposed methodology to a San Francisco Bay image acquired from an AIRSAR sensor with the number of looks equal to four [26]. Fig. 6(a) shows the adopted SAR image for the HV channel

and a particular selected image strip for analysis. Now we aim at describing the intensities of the imagery within the selected strip according to two regions: forest and ocean. Fitted data shown in Fig. 6(b)–6(d) display a qualitative comparison favorable to the BGN and GGN models, which are capable of better fitting than Γ and beta standard distributions. In particular, the proposed GGN seems to outperform the competing models. In a quantitative analysis, ML estimates involved in this application are presented in Table 4. Table 5 shows goodness-of-fit values. The GGN distribution is the best model according to all adopted criteria.

Table 4: ML estimates for the $BGN(s, \mu, \sigma, \alpha, \beta)$ [6], $GGN(a, \mu, \sigma, s)$, $\Gamma(\alpha, \beta)$ and $beta(\alpha, \beta)$ distributions. Standard errors are in parenthesis.

Model	Estimated Parameters				
<i>For the HH channel</i>					
BGN	0.665 (0.101)	4.291×10^{-2} (1.655×10^{-2})	3.240×10^{-2} (3.336×10^{-2})	1.675 (0.821)	0.188 (0.116)
GGN	2.791 (0.175)	4.283×10^{-2} (1.151×10^{-2})	1.496×10^{-3} (1.661×10^{-3})	0.304 (0.016)	• •
Γ	0.725 (0.034)	9.935 (0.637)	• •	• •	• •
beta	0.376 (0.049)	4.775 (1.041)	• •	• •	• •
<i>For the HV channel</i>					
BGN	0.713 (0.191)	1.283×10^{-2} (0.1693×10^{-2})	2.362×10^{-3} (2.741×10^{-3})	0.962 (0.292)	0.186 (0.066)
GGN	2.313 (0.128)	1.198×10^{-3} (1.647×10^{-4})	2.321×10^{-6} (7.479×10^{-6})	2.157×10^{-1} (1.595×10^{-2})	• •
Γ	0.468 (0.022)	13.152 (1.063)	• •	• •	• •
beta	0.296 (0.021)	8.020 (0.904)	• •	• •	• •
<i>For the VV channel</i>					
BGN	0.857 (0.107)	9.104×10^{-3} (2.915×10^{-3})	1.552×10^{-2} (0.291×10^{-2})	1.369 (0.793)	0.251 (0.120)
GGN	2.766 (0.403)	8.894×10^{-2} (4.375×10^{-2})	0.907×10^{-3} (1.002×10^{-3})	0.373 (0.029)	• •
Γ	0.388 (0.044)	3.929 (0.636)	• •	• •	• •
beta	0.925 (0.071)	10.280 (0.945)	• •	• •	• •

Computational cost is also quantified for both generalized models GGN and BGN. Computations were performed in a 64-bit Intel(R) Core(TM) i5-3317U CPU running at 1.70 GHz. Table 6 summarizes the average execution times in seconds. Such average times were obtained from one hundred instantiations without replacement with sample sizes of 100, 200, and 300 from selected AIRSAR region, as suggested by Efron [10]. As expected, the execution times increase according to the sample size. However, the GGN estimation could be computed faster when compared to the BGN model computation.

8 Conclusion

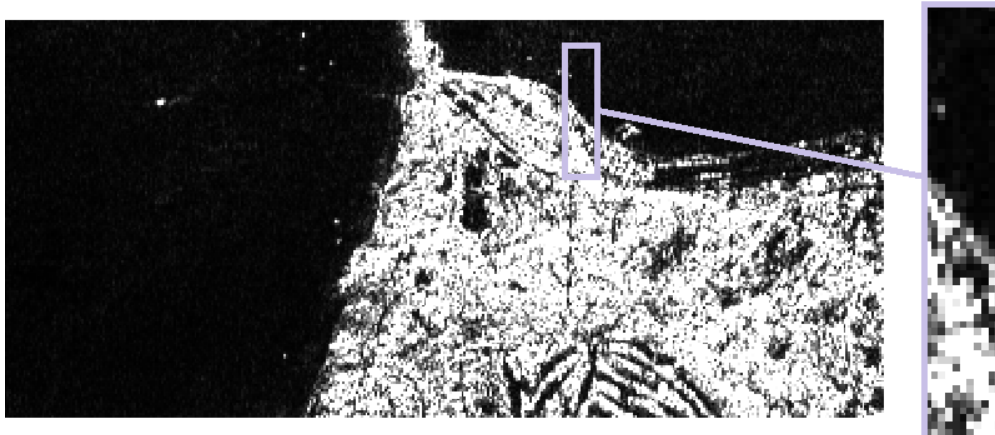
The new gamma generalized normal (GGN) distribution is proposed and discussed. Some statistical properties of the new model are investigated, such as: asymptotic behavior, density and moments, power series expansions, maximum likelihood estimation, and random number generation. The derived tools bring themselves a great potentiality in both future theoretical studies and applications as input in image post-processing

Table 5: Goodness-of-fit measures for the fitted BGN, GGN, Γ and beta distributions on AIRSAR real data

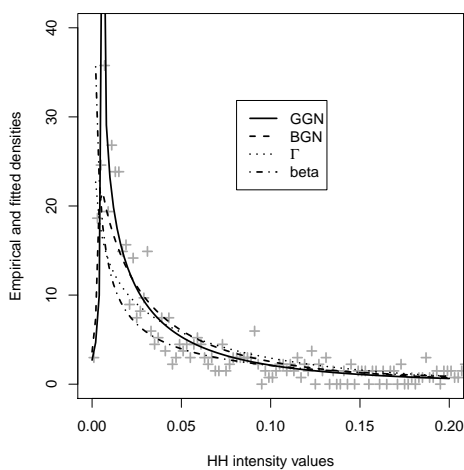
Goodness-of-fit measures	Channel	<i>Performance for different model</i>			
		GGN	BGN	Γ	beta
$d_{KL}(X)$	HH	32.440	37.960	56.361	59.518
$d_{\chi^2}(X)$		84.720	112.800	211.733	167.780
d_{KS}		4.501×10^{-2}	9.162×10^{-2}	0.125	0.206
W^*		0.312	0.791	2.307	2.610
A^*		1.772	4.506	13.458	15.189
AIC		-2.332×10^3	-2.309×10^3	-2.218×10^3	-2.055×10^3
AIC _c		-2.329×10^3	-2.307×10^3	-2.216×10^3	-2.053×10^3
BIC		-2.327×10^3	-2.306×10^3	-2.209×10^3	-2.046×10^3
$d_{KL}(X)$	HV	46.322	98.0581	79.318	67.2000
$d_{\chi^2}(X)$		108.246	263.9445	203.313	158.1546
d_{KS}		0.115	0.2187	0.175	0.2153
W^*		1.823	4.4522	3.972	3.9070
A^*		9.738	26.4101	23.514	23.2618
AIC		-3.724×10^3	-3.375×10^3	-3.489×10^3	-3.399×10^3
AIC _c		-3.722×10^3	-3.373×10^3	-3.487×10^3	-3.397×10^3
BIC		-3.719×10^3	-3.372×10^3	-3.480×10^3	-3.390×10^3
$d_{KL}(X)$	VV	14.880	21.124	26.523	36.672
$d_{\chi^2}(X)$		40.420	88.446	223.184	86.066
d_{KS}		4.468×10^{-2}	0.118	0.120	0.243
W^*		0.248	1.791	2.243	2.907
A^*		1.463	10.911	13.294	17.050
AIC		-2.009×10^3	-1.886×10^3	-1.889×10^3	-1.641×10^3
AIC _c		-2.007×10^3	-1.884×10^3	-1.887×10^3	-1.639×10^3
BIC		-2.004×10^3	-1.883×10^3	-1.880×10^3	-1.632×10^3

Table 6: Computational time (in seconds) for the fitting according to the GGN and BGN models

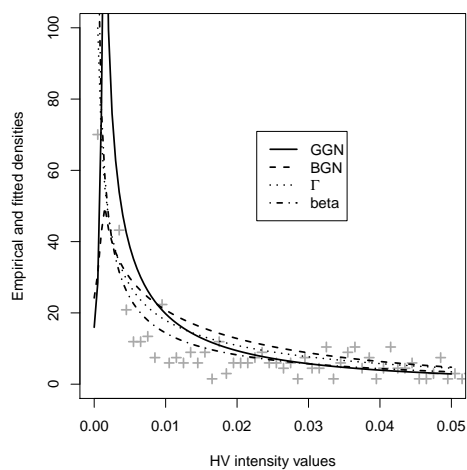
Channel	Size	GGN	BGN
HH	300	2.220	2.870
	200	1.469	2.050
	100	0.948	1.168
HV	300	2.150	2.709
	200	1.754	2.303
	100	1.108	1.239
VV	300	2.336	2.936
	200	1.582	2.058
	100	0.927	1.121



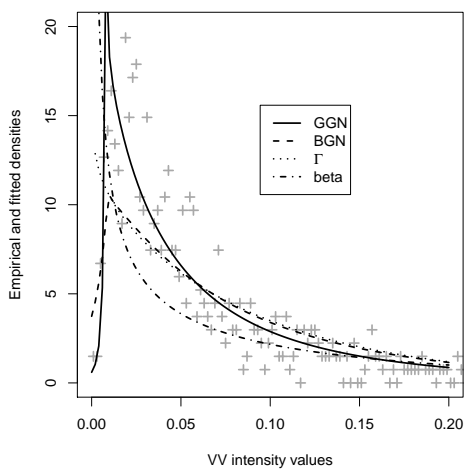
(a) AIRSAR image



(b) HH channel



(c) HV channel



(d) VV channel

Figure 6: (a) AIRSAR image with a selected strip and (b)–(d) fitted and empirical densities for the HH, HV, and VV channels, respectively.

activities:

- i) Improvement in the estimation of the shape parameter s (which imposed the more hard estimation by our synthetic results) of the proposed model by using the Mellin transform according to Gao *et al.* [16].
- ii) Retrieval of images via the gamma generalized Gaussian distributions equipped support vector machine, analogously what was proposed by Ranjani and Babu [27] and
- iii) Flexibilization of the change detection methods through the GNG model, by modifying the proposal in [34].

Importantly, evidence was found for applicability of the proposed GGN distribution in the modeling of SAR images. Real data analysis shows that the introduced model can accurately characterize SAR intensities for several polarization channels. Moreover, the GGN can outperform the beta generalized normal (BGN) distribution in terms of goodness-of-fit statistics. Bayesian restoration methods for SAR images (such as discussed in [4]) involving the GGN and BGN models is a future research line along with other post-processing steps.

Acknowledgements

The authors would like to thank the financial support of CNPq and FACEPE, Brazil. Additionally, we also would like to thank to the European Space Agency (ESA), which has distributed software and sources of datasets in form of the Polarimetric SAR Data Processing and Educational (PolSARpro) tool.

References

- [1] K. ADAMIDIS AND S. LOUKAS, *A lifetime distribution with decreasing failure rate*, *Statistics & Probability Letters*, 39 (1998), pp. 35–42.
- [2] A. AKINSETE, F. FAMOYE, AND C. LEE, *The beta-Pareto distribution*, *Statistics*, 42 (2008), pp. 547–563.
- [3] D. BLACKNELL, *Comparison of parameter estimators for K-distribution*, *IEE Proceedings-Radar, Sonar and Navigation*, 141 (1994), pp. 45–52.
- [4] C. BOUMAN AND K. SAUER, *A generalized gaussian image model for edge-preserving MAP estimation*, *IEEE Transactions on Image Processing*, 2 (1993), pp. 296–310.
- [5] V. G. CANCHO, M. DE CASTRO, AND D. K. DEY, *Long-term survival models with latent activation under a flexible family of distributions*, *Brazilian Journal of Probability and Statistics*, 27 (2013), pp. 585–600.
- [6] R. CINTRA, L. RÊGO, G. CORDEIRO, AND A. NASCIMENTO, *Beta generalized normal distribution with an application for SAR image processing*, *Statistics*, 48 (2012), pp. 1–16.
- [7] G. M. CORDEIRO, E. M. ORTEGA, AND G. O. SILVA, *The exponentiated generalized gamma distribution with application to lifetime data*, *Journal of Statistical Computation and Simulation*, 81 (2011), pp. 827–842.
- [8] Y. DELIGNON, R. GARELLO, AND A. HILLION, *Statistical modelling of ocean SAR images*, *IEE Proceedings Radar, Sonar and Navigation*, 144 (1997), pp. 348–354.
- [9] A. P. DOULGERIS, S. N. ANFINSEN, AND T. ELTOFT, *Automated non-gaussian clustering of polarimetric synthetic aperture radar images*, *IEEE Transactions on Geoscience and Remote Sensing*, 49 (2011), pp. 3665–3676.
- [10] B. EFRON, *More efficient bootstrap computations*, *Journal of the American Statistical Association*, 85 (1990), pp. 79–89.

- [11] S. EGUCHI AND J. COPAS, *Interpreting Kullback-Leibler divergence with the Neyman-Pearson lemma*, Journal of Multivariate Analysis, 97 (2006), pp. 2034–2040.
- [12] A. EL-ZAART AND D. ZIOU, *Statistical modelling of multimodal SAR images*, International Journal of Remote Sensing, 28 (2007), pp. 2277–2294.
- [13] D. L. EVANS, J. H. DREW, AND L. M. LEEMIS, *The distribution of the Kolmogorov-Smirnov, Cramer-von Mises, and Anderson-Darling test statistics for exponential populations with estimated parameters*, Communications in Statistics - Simulation and Computation, 37 (2008), pp. 1396–1421.
- [14] A. C. FRERY, H. J. MULLER, C. C. F. YANASSE, AND S. J. S. SANT’ANNA, *A model for extremely heterogeneous clutter*, IEEE Transactions on Geoscience and Remote Sensing, 35 (1997), pp. 648–659.
- [15] G. GAO, *Statistical modeling of SAR images: A survey*, Sensors, 10 (2010), pp. 775–795.
- [16] G. GAO, G. LI, AND Y. LI, *Shape parameter estimator of the generalized gaussian distribution based on the MoLC*, IEEE Geoscience and Remote Sensing Letters, 15 (2018), pp. 350–354.
- [17] R. GUPTA, P. GUPTA, AND R. GUPTA, *Modeling failure time data by Lehman alternatives.*, Communications in Statistics—Theory and Methods, 27 (1998), pp. 887–904.
- [18] R. GUPTA AND D. KUNDU, *Generalized exponential distributions*, Australian and New Zealand Journal of Statistics, 41 (1999), pp. 173–188.
- [19] C. D. LAI, *Constructions and applications of lifetime distributions*, Applied Stochastic Models in Business and Industry, 29 (2013), pp. 127–140.
- [20] J. S. LEE AND E. POTTIER, *Polarimetric Radar Imaging: From Basics to Applications*, CRC, Boca Raton, 2009.
- [21] G. MUDHOLKAR AND D. SRIVASTAVA, *Exponentiated weibull family for analyzing bathtub failure-rate data*, IEEE Transactions on Reliability, 42 (1993), pp. 299–302.
- [22] G. S. MUDHOLKAR, D. K. SRIVASTAVA, AND M. FREIMER, *The exponentiated weibull family: A reanalysis of the bus-motor-failure data*, Technometrics, 37 (1995), pp. 436–445.
- [23] S. NADARAJAH, *A generalized normal distribution*, Journal of Applied Statistics, 32 (2005), pp. 685–694.
- [24] S. NADARAJAH, G. M. CORDEIRO, AND E. M. M. ORTEGA, *The gamma-G family of distributions: Mathematical properties and applications*, Journal of Statistical Computation and Simulation, (2013).
- [25] S. NADARAJAH AND A. GUPTA, *The exponentiated gamma distribution with application to drought data*, Calcutta Statistical Association Bulletin, 59 (2007), pp. 29–54.
- [26] A. D. C. NASCIMENTO, M. M. HORTA, A. C. FRERY, AND R. J. CINTRA, *Comparing edge detection methods based on stochastic entropies and distances for PolSAR imagery*, IEEE Journal of Selected Topics in Applied Earth Observations and Remote Sensing, 7 (2014), pp. 648–663.
- [27] J. J. RANJANI AND M. BABU, *Image retrieval using generalized gaussian distribution and score based support vector machine*, Indian Journal of Science and Technology, 9 (2016).
- [28] M. M. RISTIĆ AND N. BALAKRISHNAN, *The gamma-exponentiated exponential distribution*, Journal of Statistical Computation and Simulation, 82 (2012), pp. 1–16.
- [29] S. ROSS, *Simulation*, Academic Press, 2006.
- [30] A. K. SEGHOUANE AND S. I. AMARI, *The AIC criterion and symmetrizing the Kullback-Leibler divergence*, IEEE Transactions on Neural Networks, 18 (2007), pp. 97–106.
- [31] R. B. SILVA, M. BOURGUIGNON, AND G. M. CORDEIRO, *A new compounding family of distributions: The generalized gamma power series distributions*, Journal of Computational and Applied Mathematics, 303 (2016), pp. 119 – 139.
- [32] I. J. TANEJA, *Bounds on triangular discrimination, harmonic mean and symmetric chi-square divergences*, Journal of Concrete and Applicable Mathematics, 4 (2006), pp. 91–111.
- [33] Q. H. VUONG, *Likelihood ratio tests for model selection and non-nested hypotheses*, Econometrica, 57 (1989), pp. 307–333.
- [34] F. M. YAKOUB BAZI, LORENZO BRUZZONE, *Change detection in multitemporal sar images based on generalized gaussian distribution and em algorithm*, 2004.
- [35] K. ZOGRAFOS AND N. BALAKRISHNAN, *On families of beta- and generalized gamma-generated distributions and associated inference*, Statistical Methodology, 6 (2009), pp. 344 – 362.